

Synthesis and Design of Generalized Chebyshev Wideband Hybrid Ring Based Bandpass Filters With a Controllable Transmission Zero Pair

Jian-Yu Li, *Student Member, IEEE*, Chun-Hsiang Chi, and Chi-Yang Chang, *Member, IEEE*

Abstract—A systematic and analytical method for the exact synthesis of generalized Chebyshev wideband hybrid ring based bandpass filters with a controllable transmission zero pair is developed in this paper. The basic configuration of the proposed filters consists of a hybrid ring, a multi-section short-circuited stub and a multi-section open-circuit stub. In this configuration, the position of the controllable transmission zero pair can be easily designed by setting the impedances of the multi-section short-circuited stub and the multi-section open-circuit stub. According to the position of the controllable transmission zero pair, two kinds of filters are proposed. The filter has a controllable transmission zero pair on the real axis (imaginary frequency) that they can be arranged to improve the group delay flatness. On the other hand, the filter has a controllable transmission zero pair on the imaginary axis (real frequency) and the desired stopband suppression can be obtained by adjusting the optimal position of them. This synthesis method is developed to obtain the impedance value of each line section and ripple factors of the filters with respect to given specifications (center frequency, passband bandwidth and transmission zeros). Two design examples, the fifth-order filter with a controllable imaginary frequency transmission zero pair and the fifth-order filter with a controllable real frequency transmission zero pair, are synthesized and fabricated. The measured results validate and confirm the theoretical predictions.

Index Terms—Generalized Chebyshev response, hybrid ring based bandpass filter, hybrid ring, phase inverter, wideband bandpass filter.

I. INTRODUCTION

THE microwave filter is a key element in the majority of RF systems supporting modern telecommunication services. Recently, some broadband systems such as ultra-wideband radar and high data-rate communication system require broadband, highly selective and low loss microwave passive filters. Therefore, the design of a wideband bandpass filter has become an important issue. In order to meet this trend, wideband bandpass filters have been recently developed based on various methodologies. For examples, in [1] and [2], wide bandwidth filters

were implemented by a direct cascade of the low- and high-pass filters. In [1], wideband coplanar waveguide bandpass filters based on the cascade of coplanar waveguide low- and high-pass periodic structures were constructed. To save the circuit area, wideband bandpass filters were proposed by combining the low and high-pass filters together [2]. These wideband filters have a good suppression on the out-of-band response while they have a drawback of the large circuit size. In [3], a bandpass filter with an increased bandwidth obtained from a resonator coupling enhancement with three-line coupling sections was reported. In [4], the parallel-coupled microstrip line with patterned ground was employed to give a tight coupling for a wideband bandpass filter. However, in [3] and [4], to obtain wider bandwidth, the smaller gap size is demanded to enhance the coupling. This small gap may cause some difficulties in the fabrication processes. The wideband bandpass filter constructed using the multiple-mode resonator was initially proposed in [5]. Later on, various multiple-mode resonator based wideband bandpass filters have been implemented in microstrip, coplanar-waveguide, slotline, as well as many other hybrid structures [6], [7]. Another class of ring-based wideband bandpass filters was illustrated in [8]–[12]. They need to cascade two or more rings to meet the desired features and still increase the circuitry area. Although growing numbers of wideband bandpass filters have been reported, most of them are usually designed relying on the cut-and-try approach by using the commercial software. As a result, it is necessary to develop a systematic synthesis approach to design a wideband bandpass filter. Nevertheless, only few works address this issue, such as [12]–[15]. In [12], the wideband bandpass filter by cascading of two 180° hybrid rings is synthesized based on the insertion loss function of Chebyshev response [16]. In [13], the proposed synthesis method can be used to analyze the wideband bandpass filter comprising high-pass, low-pass and isolation sections. In [14], the wideband bandpass filter with composite series and shunt stubs can be synthesized by the developed synthesis approach based on [17]–[19]. The wideband bandpass filter using $3/4$ wavelength parallel-coupled line resonators presented in [15] is also synthesized based on [19].

Thus, in this paper, a rigorous theoretical analysis of the proposed generalized Chebyshev wideband hybrid ring based bandpass filters with a controllable transmission zero pair is carried out and the proposed filters can be achieved without any tight coupling scheme. The schematic diagrams of proposed filters are depicted in Fig. 1. Fig. 1(a) shows the filter with a controllable imaginary frequency transmission zero pair while Fig. 1(b) shows the filter with a controllable real frequency transmission zero pair. The controllable transmission zero pair can be used to

Manuscript received June 05, 2010; revised August 21, 2010; accepted August 30, 2010. Date of publication November 01, 2010; date of current version December 10, 2010. This work was supported in part by the National Science Council, Taiwan, under Grant NSC 98-2221-E-009-034-MY3 and Grant NSC 99-2221-E-009-050-MY3.

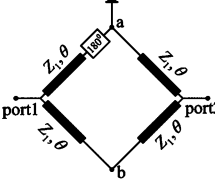
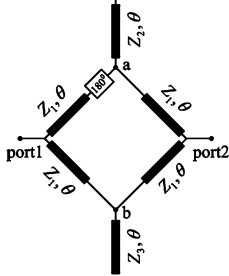
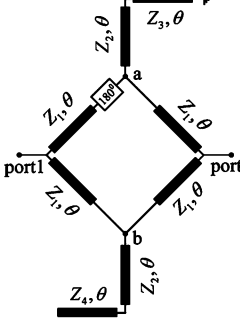
J. Y. Li and C. Y. Chang are with the Department of Communication Engineering, National Chiao Tung University, Hsinchu 300, Taiwan (e-mail: JianYu@itri.org.tw; mhchang@cc.nctu.edu.tw).

C. H. Chi is with the Information and Communications Laboratories, ITRI, Hsinchu 310, Taiwan (e-mail: chschi@itri.org.tw).

Color versions of one or more of the figures in this paper are available online at <http://ieeexplore.ieee.org>.

Digital Object Identifier 10.1109/TMTT.2010.2083930

TABLE I
 STRUCTURES AND CHARACTERISTICS OF FILTERS WITH A CONTROLLABLE IMAGINARY FREQUENCY TRANSMISSION ZERO PAIR

1. PROPOSED FILTER STRUCTURE			
2. Filter order	3	5	7
3. Roots of $S_{21}^{cir}(Z_1, Z_2, \dots, Z_i, \tan \theta) = 0$	$\tan \theta_z = \{0, \pm j\}$	$\tan \theta_z = \left\{ 0, \pm j, \pm \sqrt{\frac{Z_3}{Z_2}} j \right\}$	$\tan \theta_z = \left\{ 0, \pm j, \pm j, \pm \sqrt{\frac{Z_4}{Z_3}} j \right\}$
4. Finite-frequency transmission zeros in lowpass domain $\Omega_z = \delta \cdot (\tan \theta_z)^{-1}$	$\Omega_z = \left\{ \frac{\delta}{\pm j} \right\}$	$\Omega_z = \left\{ \frac{\delta}{\pm j}, \frac{\delta}{\pm j}, \frac{\delta}{\pm \sqrt{\frac{Z_3}{Z_2}} j} \right\}$	$\Omega_z = \left\{ \frac{\delta}{\pm j}, \frac{\delta}{\pm j}, \frac{\delta}{\pm \sqrt{\frac{Z_4}{Z_3}} j} \right\}$

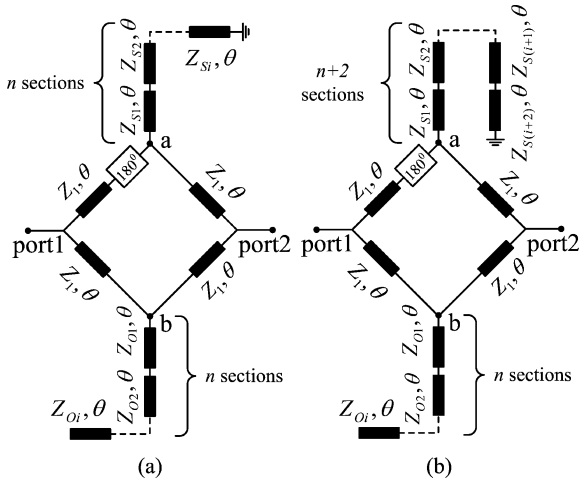


Fig. 1. Proposed wideband bandpass filters with (a) a controllable imaginary frequency transmission zero pair and (b) a controllable real frequency transmission zero pair.

flatten the group delay or improve the selectivity. In the meantime, a synthesis approach is developed to design the proposed filters in the closed-form format following the studies of [20] and [21]. Based on the developed synthesis approach, once the positions of the transmission zeros and the fractional bandwidth are chosen, the impedance of each line section, as well as the passband ripple level of the proposed filters can be exactly determined. The procedure is applied to synthesize a fifth-order filter with a controllable transmission zero pair on the imaginary frequency and a fifth-order filter with a controllable transmission zero pair on the real frequency. Both design examples are implemented using finite ground coplanar waveguide and coplanar stripline on an Al_2O_3 substrate and the measured data confirms the validity of the proposed method.

II. DESIGN AND SYNTHESIS PROCEDURE

The systematic design procedure can be summarized into four steps and the detailed description of each step is discussed in the following:

A. Step1-Prototypes and Characteristics of Proposed Filters

The proposed filters are depicted in Fig. 1(a) and (b) respectively. Each line section is commensurate with the electrical length θ of 90 degree at the center frequency.

The filter with a controllable transmission zero pair on the imaginary frequency, as shown in Fig. 1(a), is composed of a hybrid ring, an n -section short-circuited stub and an n -section open-circuited stub. The impedances for that short-circuited and open-circuited stub are labeled as Z_{Si} and Z_{Oi} , where i indicates the i -th section of the stub. Meanwhile, the relation of impedances between these two stubs is $Z_{S1} = Z_{O1}, Z_{S2} = Z_{O2} \dots, Z_{S(i-1)} = Z_{O(i-1)}$ and $Z_{Si} \neq Z_{Oi}$. Besides, the order of the filter with a controllable imaginary frequency transmission zero pair is $(2i + 3)$. This result implies that a higher order filter can be achieved by increasing more sections for the short-circuited and open-circuited stub. As shown in Table I, when i equals to 0, 1, and 2, corresponding to third-, fifth-, and seventh-order filter respectively.

On the other hand, Fig. 1(b) depicts the filter with a controllable transmission zero pair on the real frequency that it comprises a hybrid ring, an $(n + 2)$ -section short-circuited stub, and an n -section open-circuited stub. The impedances for that short-circuited and open-circuited stub are also labeled as Z_{Si} and Z_{Oi} , and the relation of impedances between that two stubs is $Z_{S1} = Z_{O1}, Z_{S2} = Z_{O2} \dots, Z_{Si} = Z_{Oi}$. Moreover, the impedance $Z_{S(i+1)}$ and $Z_{S(i+2)}$ are related to the position of transmission zeros and this issue will be examined later. The

TABLE II
STRUCTURES AND CHARACTERISTICS OF FILTERS WITH A CONTROLLABLE REAL FREQUENCY TRANSMISSION ZERO PAIR

1. PROPOSED FILTER STRUCTURE			
2. Filter order	5	7	9
3. Roots of $S_{21}^{cir}(Z_1, Z_2, \dots, Z_i, \tan \theta) = 0$	$\tan \theta_z = \left\{ 0, \pm j, \pm \sqrt{\frac{Z_2}{Z_3}} \right\}$	$\tan \theta_z = \left\{ 0, \pm j, \pm j, \pm \sqrt{\frac{Z_3}{Z_4}} \right\}$	$\tan \theta_z = \left\{ 0, \pm j, \pm j, \pm j, \pm \sqrt{\frac{Z_4}{Z_5}} \right\}$
4. Finite-frequency transmission zeros in lowpass domain $\Omega_z = \delta \cdot (\tan \theta_z)^{-1}$	$\Omega_z = \left\{ \frac{\delta}{\pm j}, \frac{\delta}{\pm \sqrt{\frac{Z_2}{Z_3}}} \right\}$	$\Omega_z = \left\{ \frac{\delta}{\pm j}, \frac{\delta}{\pm j}, \frac{\delta}{\pm \sqrt{\frac{Z_3}{Z_4}}} \right\}$	$\Omega_z = \left\{ \frac{\delta}{\pm j}, \frac{\delta}{\pm j}, \frac{\delta}{\pm j}, \frac{\delta}{\pm \sqrt{\frac{Z_4}{Z_5}}} \right\}$

order of the filter with a controllable real frequency transmission zero pair is $(2i + 5)$. It also implies that the more sections of short-circuited and open-circuited stub are used, the higher order filter can be obtained. Refer to Table II, the fifth-, seventh-, and ninth-order filter corresponds to i value of 0, 1 and 2 respectively.

Because of its symmetrical property, the proposed structures can be analyzed by even- and odd-mode analysis. For the even-mode excitation, the corresponding reflection coefficient Γ_{even} can be obtained from the even-mode eigennetwork. Similarly, the reflection coefficient Γ_{odd} can be derived from the odd-mode eigennetwork. Therefore, S_{11} and S_{21} of the filter can be obtained as

$$S_{11}^{\text{cir}} = (\Gamma_{\text{even}} + \Gamma_{\text{odd}})/2 = f(Z_1, Z_2, \dots, \tan \theta) \quad (1)$$

$$S_{21}^{\text{cir}} = (\Gamma_{\text{even}} - \Gamma_{\text{odd}})/2 = f(Z_1, Z_2, \dots, \tan \theta) \quad (2)$$

where $\Gamma_{\text{even}}, \Gamma_{\text{odd}}, S_{11}^{\text{cir}}$ and S_{21}^{cir} are the function of electrical length θ and the impedance of each line section. The roots of $S_{21}^{\text{cir}} = 0$ are $\tan \theta_z = r_1, r_2, \dots, r_n$, where r_1, r_2, \dots, r_n are related to the impedance of each line section. The roots which can be mapped to the finite-frequency transmission zeros in the lowpass domain are listed in Table I and Table II.

B. Step 2-Lowpass-to-Bandpass Transformation

Consider the frequency transformation for the design of the proposed filter. Fig. 2 shows the typical frequency response $|S_{21}|$ of the filter in two frequency domains. Domain ω is the actual frequency where the bandpass filter operates, and the Ω

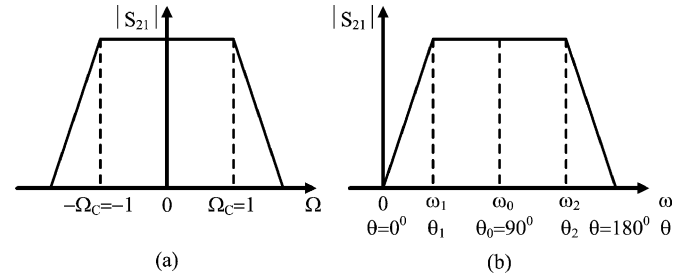


Fig. 2. Frequency response of (a) lowpass domain and (b) bandpass domain.

is a normalized frequency for the lowpass prototype. In our design, the lowpass prototype can be transformed to the bandpass prototype through the frequency mapping function

$$\Omega = -\delta \cdot (\tan \theta)^{-1}, \quad \theta = \frac{\pi}{2} \cdot \frac{\omega}{\omega_0} \quad (3)$$

where ω_0 is the center frequency of the bandpass filter and δ is the scaling factor used for the lowpass-to-bandpass transformation. In (3), the parameter δ needs to be determined. In Fig. 2, the low-pass cutoff frequencies $-\Omega_C$ and Ω_C should be mapped to the lower and upper cutoff frequencies ω_1 and ω_2 of the bandpass filter. Then, the frequency mapping functions of $-\Omega_C$ and Ω_C in terms of ω_1 and ω_2 are

$$-\delta \cdot \cot \left(\frac{\pi}{2} \cdot \frac{\omega_1}{\omega_0} \right) = -\Omega_C = -1 \quad (4)$$

$$-\delta \cdot \cot \left(\frac{\pi}{2} \cdot \frac{\omega_2}{\omega_0} \right) = \Omega_C = 1. \quad (5)$$

Since ω_0 is the center frequency of ω_1 and ω_2 , given by $\omega_0 = (\omega_1 + \omega_2)/2$; we can obtain

$$\begin{aligned} \delta \cdot \cot\left(\frac{\pi}{2} \cdot \frac{2\omega_1}{\omega_1 + \omega_2}\right) &= \delta \cdot \tan\left[\frac{\pi}{2} \left(1 - \frac{2\omega_1}{\omega_1 + \omega_2}\right)\right] \\ &= \delta \cdot \tan\left(\frac{\pi}{2} \cdot \frac{\omega_2 - \omega_1}{\omega_1 + \omega_2}\right) = 1 \end{aligned} \quad (6)$$

$$\begin{aligned} \delta \cdot \cot\left(\frac{\pi}{2} \cdot \frac{2\omega_2}{\omega_1 + \omega_2}\right) &= \delta \cdot \tan\left[\frac{\pi}{2} \left(1 - \frac{2\omega_2}{\omega_1 + \omega_2}\right)\right] \\ &= \delta \cdot \tan\left(\frac{\pi}{2} \cdot \frac{\omega_1 - \omega_2}{\omega_1 + \omega_2}\right) = -1. \end{aligned} \quad (7)$$

Both (6) and (7) give the value of δ

$$\delta = \frac{1}{\tan\left(\frac{\pi}{2} \cdot \frac{\omega_2 - \omega_1}{\omega_1 + \omega_2}\right)} = \frac{1}{\tan\left(\frac{\pi}{2} \cdot \frac{W}{2 \cdot \omega_0}\right)} \quad (8)$$

where $W = \omega_2 - \omega_1$ is the passband bandwidth of the filter. By substituting (8) into (3), the complete frequency mapping function are represented as

$$\Omega = -\frac{1}{\tan\left(\frac{\pi}{2} \cdot \frac{W}{2 \cdot \omega_0}\right)} \cdot (\tan \theta)^{-1} \quad (9)$$

As a result, the finite-frequency transmission zeros in lowpass domain are obtained as

$$\begin{aligned} \Omega_z &= -\delta \cdot (\tan \theta_z)^{-1} \\ &= \{-\delta \cdot r_1^{-1}, -\delta \cdot r_2^{-1}, \dots, -\delta \cdot r_n^{-1} | n \in N\} \end{aligned} \quad (10)$$

where $\tan \theta_z$ is the solution set of $S_{21}^{\text{cir}} = 0$ as described in Step 1. The lowpass domain transmission zeros for both kinds of filters are depicted in the fourth row of Tables I and II.

For the filters shown in Table I, all the transmission zero pairs are located on the real axis (imaginary frequency) and only one pair of them are controllable as long as the order of the filter is greater than three. The positions of this controllable transmission zero pair are determined by the impedance ratio of the last section of the open-circuited and short-circuited stubs, namely Z_{O_i} and Z_{S_i} . The locations of this controllable transmission pair can be adjusted to improve the group delay flatness.

Similarly, the filters shown in Table II have a single controllable transmission zero pair on the imaginary axis (real frequency) and the others are on the real axis (imaginary frequency). The position of this controllable transmission zero pair is determined by the impedance ratio of the last two sections of the short-circuited stub, namely $Z_{S(i+1)}$ and $Z_{S(i+2)}$. Therefore, the designer can arbitrarily assign a pair of transmission zeros in the real frequency to improve the selectivity.

C. Step3-Synthesize Generalized Chebyshev Filter Function

In this paper, the generalized Chebyshev filter function in the lowpass domain can be obtained by adopting the method proposed by R. J. Cameron [20]. Cameron developed an efficient recursive technique to generate the generalized Chebyshev

transfer and reflection polynomials with arbitrarily distributed transmission zeros. The generalized Chebyshev filter functions are in the form

$$S_{11}(\Omega) = \frac{F(\Omega)/\varepsilon_R}{E(\Omega)} \quad (11)$$

$$S_{21}(\Omega) = \frac{P(\Omega)/\varepsilon}{E(\Omega)} \quad (12)$$

$$\varepsilon = \frac{1}{\sqrt{10^{L_R/10} - 1}} \cdot \left| \frac{P(\Omega)}{F(\Omega)/\varepsilon_R} \right|_{\Omega=\pm 1} \quad (13)$$

where L_R is the prescribed return loss level in decibels, ε_R is unity for all cases except fully canonical filtering functions. The polynomials $P(\Omega)$, $F(\Omega)$ and $E(\Omega)$ have been normalized with the coefficient of each highest degree term to be unity. Both $E(\Omega)$ and $F(\Omega)$ are N th-degree polynomials, N is the order of filter, while $P(\Omega)$ is the polynomial of degree n_{fz} , where n_{fz} is the number of finite-frequency transmission zeros.

Summarizing the Cameron's method, the polynomial $F(\Omega)$ can be obtained by the last cycle of this recursion method, and the polynomial $P(\Omega) = \prod_{n=1}^{n_{fz}} (\Omega - \Omega_n)$ is determined by the finite-frequency transmission zeros in the lowpass domain. Hence, the polynomial $E(\Omega)$ can be constructed by finding the zeros of the polynomial $P(\Omega)/\varepsilon - jF(\Omega)/\varepsilon_R$ with the alternating singularity principle. Actually, only $P(\Omega)$ and $F(\Omega)$ are utilized in this paper and the reason will be examined later. It should be noted that the ripple factor ε is a variable in this paper. That is, the generalized Chebyshev transfer and reflection polynomials are the function of the ripple factor ε .

D. Step4-Obtain Parameters of Proposed Filters

The final step is to use the equal-ripple approximating function [16] to obtain parameters of the proposed filters. Because the proposed filters are symmetrical and lossless, this function is useful to analyze such problems. The form of the equal-ripple approximating function is acquired by taking S_{11} over S_{21} or jS_{21} . If S_{11}/S_{21} or S_{11}/jS_{21} is a pure real function and equal ripple, we can ensure that magnitude of S_{11} will be equal ripple as desired. From (1), (2), (11) and (12), we have two equal-ripple approximating functions. It should be noted that (11) and (12) need to be translated to the bandpass domain. If these two functions are equal, as expressed in (14), the ripple factor and the impedance corresponding to each line section can be obtained

$$\frac{S_{11}(\tan \theta)}{S_{21}(\tan \theta)} = \frac{P(\tan \theta)}{\varepsilon \cdot F(\tan \theta)} = \frac{S_{11}^{\text{cir}}(\tan \theta)}{j \cdot S_{21}^{\text{cir}}(\tan \theta)}. \quad (14)$$

Here, all the above-described design procedures can be summarized into a flow chat shown in Fig. 3.

III. SYNTHESIS AND SIMULATION OF PROPOSED FILTERS

The systematic synthesis method described in Section II is validated here with two design examples and the other related discussions are also presented.

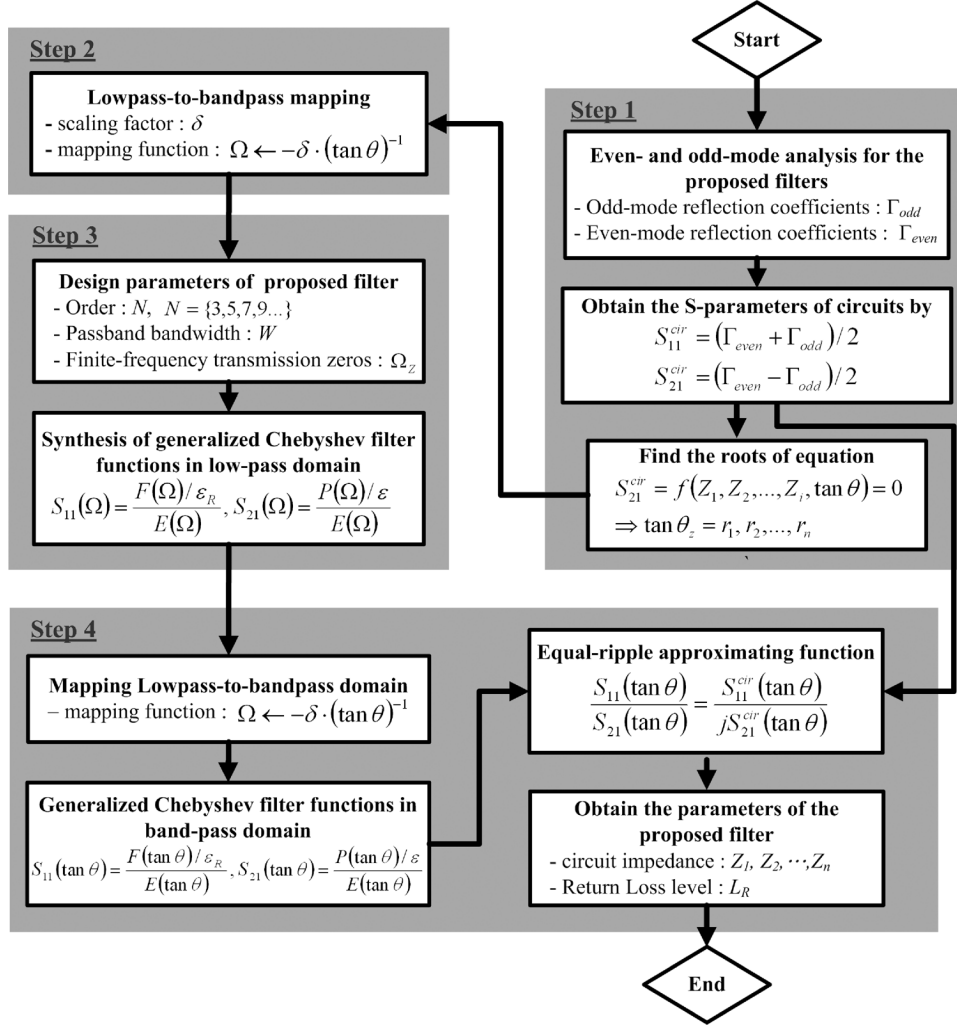


Fig. 3. Design flow chart for the proposed filters.

A. Design Example of the Filter With a Controllable Transmission Zero Pair on the Imaginary Frequency

This design example considers a wideband bandpass filter with the following specifications.

- 1) The fifth-order Chebyshev response with all finite transmission zeros on the imaginary frequency.
- 2) Center frequency, ω_0 : 3 GHz
- 3) Passband bandwidth, W : 3 GHz (1.5–4.5 GHz)

The filter configuration is shown in the center column of Table I. In the first step, the even- and odd-mode analysis is applied to obtain the S -parameters of the filter. The even- and odd-mode eigennetworks are shown in Fig. 4, and the

reflection coefficients for the even- and odd-mode are given by

$$\Gamma_{\text{even}} = \frac{z_1^2 t^3 + j2(z_1 + z_3) \cdot t^2 - 2z_1 z_3 t - j2z_3}{z_1^2 t^3 - j2(z_1 + z_3) \cdot t^2 - 2z_1 z_3 t + j2z_3} \quad (15)$$

$$\Gamma_{\text{odd}} = \frac{-j2z_2 t^2 + (z_1^2 + 2z_1 z_2) \cdot t + j2(z_1 + z_2)}{j2z_2 t^2 + (z_1^2 + 2z_1 z_2) \cdot t - j2(z_1 + z_2)} \quad (16)$$

where $t = \tan \theta$ and z_1, z_2 and z_3 are the normalized impedance of Z_1, Z_2 and Z_3 . On the basis of the (1) and (2), the S -parameters of the filter can be expressed as (17) and (18), shown at the bottom of this page. By solving $S_{21}^{\text{cir}} = 0$, the roots can be found as follows:

$$\tan \theta_z = \{0, j, -j, j\sqrt{k}, -j\sqrt{k}\} \text{ where } k = \frac{z_3}{z_2}. \quad (19)$$

$$S_{11}^{\text{cir}} = \frac{[-4(z_1 + z_2) + 2(2z_1(z_1 + z_2) - z_3(z_1 + 2z_2)(z_1^2 - 2)) \cdot t^2 + (z_1^4 - 4z_1 z_2 + 2z_3^3 z_2 - 4z_2 z_3) \cdot t^4]}{[4z_3(z_1 + z_2) + j2z_1 z_3(3z_1 + 4z_2) \cdot t - 2(z_1^3 z_3 + 2z_2 z_3 + 2z_1^3 z_2 z_3 + 2z_1(z_1 + z_3) + 2z_2(z_1 + z_3)) \cdot t^2 - j2z_1(z_1^2 + z_1 z_2 + 2z_2 z_3 + 2z_1(z_1 + z_3) + 2z_2(z_1 + z_3)) \cdot t^3 + (z_1^4 + 2z_1^3 z_2 + 4z_2(z_1 + z_3)) \cdot t^4 + j2z_1^2 z_2 t^5]} \quad (17)$$

$$S_{21}^{\text{cir}} = \frac{j2z_1^2 z_3 t + j2z_1^2(z_2 + z_3) \cdot t^3 + j2z_1^2 z_2 t^5}{[4z_3(z_1 + z_2) + j2z_1 z_3(3z_1 + 4z_2) \cdot t - 2(z_1^3 z_3 + 2z_2 z_3 + 2z_1^3 z_2 z_3 + 2z_1(z_1 + z_3) + 2z_2(z_1 + z_3)) \cdot t^2 - j2z_1(z_1^2 + z_1 z_2 + 2z_2 z_3 + 2z_1(z_1 + z_3) + 2z_2(z_1 + z_3)) \cdot t^3 + (z_1^4 + 2z_1^3 z_2 + 4z_2(z_1 + z_3)) \cdot t^4 + j2z_1^2 z_2 t^5]} \quad (18)$$

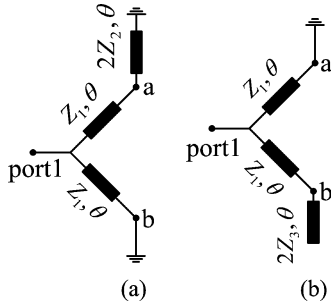


Fig. 4. (a) Odd-mode and (b) even-mode eigennetwork of the fifth-order filter with a controllable imaginary frequency transmission zero pair.

In the second step, according to the design specifications, the scaling factor and frequency mapping function can be acquired. In (8) and (9), the scaling factor $\delta = 1$ and the mapping function can be expressed as

$$\Omega = -(\tan \theta)^{-1}. \quad (20)$$

By using of (10) and (19), the finite-frequency transmission zeros in the lowpass domain can be obtained as

$$\Omega_Z = \left\{ \frac{1}{j}, \frac{1}{-j}, \frac{1}{j\sqrt{k}}, \frac{1}{-j\sqrt{k}} \right\}. \quad (21)$$

In (21), it is observed that impedance ratio k can be used to manipulate the position of transmission zeros.

In the third step, applying the Cameron's method with transmission zero locations in (21), the polynomials $P(\Omega)$ and $F(\Omega)$ can be obtained as follows:

$$P(\Omega) = \frac{1}{k} + \frac{k+1}{k}\Omega^2 + \Omega^4 \quad (22)$$

$$F(\Omega) = \frac{C(k)}{A(k)} \cdot \Omega + \frac{B(k)}{A(k)} \cdot \Omega^3 + \Omega^5 \quad (23)$$

where

$$A(k) = 11.67 + 5.83k + 11.67\sqrt{1+k} \quad (24)$$

$$B(k) = -13.49 - 3.83k - 13.66\sqrt{1+k} \quad (25)$$

$$C(k) = 3.83 + 2\sqrt{1+k}. \quad (26)$$

After the frequency mapping, (22) and (23) can be translated to the bandpass domain and expressed as

$$P(t) = \frac{1}{k} + \frac{k+1}{k} \cdot \frac{1}{t^2} + \frac{1}{t^4} \quad (27)$$

$$F(t) = \frac{C(k)}{A(k)} \cdot \frac{1}{t} + \frac{B(k)}{A(k)} \cdot \frac{1}{t^3} + \frac{1}{t^5}. \quad (28)$$

TABLE III
ANALYTICAL SOLUTIONS FOR VARIOUS k VALUES OF THE FIFTH-ORDER FILTER WITH A CONTROLLABLE IMAGINARY FREQUENCY TRANSMISSION ZERO PAIR

k	Ω_Z	Z_1 (Ohm)	Z_2 (Ohm)	Z_3 (Ohm)	ε	L_R (dB)
1.00	$\pm j1$	70.83	65.40	65.40	2.72	21.97
1.24	$\pm j0.9$	69.43	55.30	68.57	2.59	21.11
1.56	$\pm j0.8$	67.90	46.36	72.33	2.48	20.20
2.04	$\pm j0.7$	66.07	37.88	77.28	2.38	19.17
2.78	$\pm j0.6$	63.96	30.15	83.83	2.30	18.02

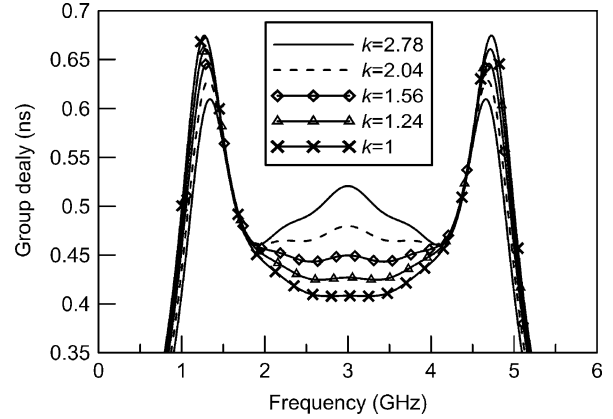


Fig. 5. Predicted performance of group delay under varied impedance ratio k .

In the fourth step, by (17), (18), (27) and (28), the two equal-ripple approximating functions can be illustrated as (29) and (30) shown at the bottom of this page.

From (14), setting (29) to be equal to (30), a polynomial equation can be obtained. This polynomial equation is with the variable t ($t = \tan \theta$) and each coefficient of the polynomial is a function of impedances and ripple factor ε . Setting each coefficient of the polynomial to be zero, the following equations can be acquired as (31), shown at the bottom of this page. According to (21) and (31), as long as the impedance ratio k is given, the line impedances $Z_1 Z_2 Z_3$, the locations of the controllable transmission zero pair Ω_Z , and the ripple factor ε can be solved. Shown in Table III are five analytical solutions according to various k values. The group delay responses corresponding to these k values are illustrated in Fig. 5. It is observed in Fig. 5 that the maximum flat group delay can be achieved by choosing the k value of 1.56. Moreover, for a fixed value

$$\frac{S_{11}^{\text{cir}}(t)}{j \cdot S_{21}^{\text{cir}}(t)} = \frac{[4(z_1 + z_2) - 2(2z_1(z_1 + z_2) - z_3(z_1 + 2z_2)(z_1^2 - 2))] \cdot t^2 - (z_1^4 - 4z_1z_2 + 2z_1^3z_2 - 4z_2z_3) \cdot t^4}{2z_1^2z_3t + 2z_1^2(z_2 + z_3) \cdot t^3 + 2z_1^2z_2t^5} \quad (29)$$

$$\frac{S_{11}(t)}{S_{21}(t)} = \frac{k\varepsilon A(k) + k\varepsilon B(k) \cdot t^2 + k\varepsilon C(k) \cdot t^4}{kA(k) \cdot t + (1+k)A(k) \cdot t^3 + A(k) \cdot t^5} \quad (30)$$

$$\begin{cases} 2(z_1 + z_2) - z_1^2\varepsilon = 0 \\ -2k \cdot [(1+k)B(k) + kC(k)]z_1^2z_2\varepsilon - A(k) \cdot \left\{ kz_1^4 + 4(1+k^2)z_1z_2 - 2k^2z_1^3z_2 + 4k(1+k)z_2^2 \right\} \\ + 2z_1^2\{2 + k[2 + z_2(\varepsilon - 2z_2(1+k))]\} \\ A(k) \cdot \{4kz_2^2(z_1^2 + k - 1) - 2z_1^3z_2 - z_1^2[4 + (1+k)z_1^2]\} - 2k \cdot [B(k) + C(k) + kC(k)] \cdot z_1^2z_2\varepsilon = 0 \end{cases} \quad (31)$$

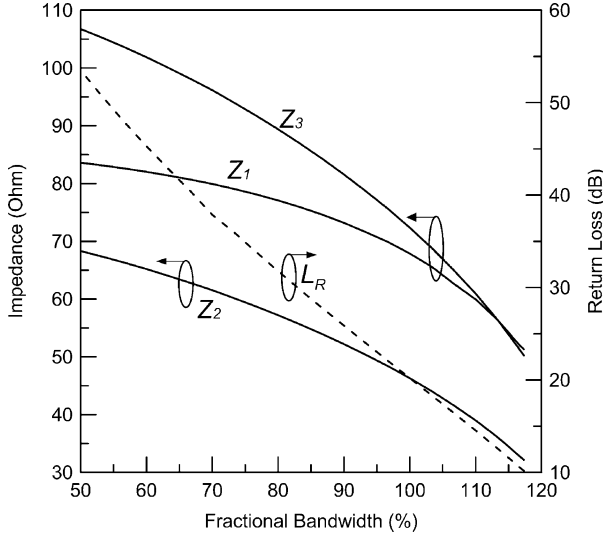


Fig. 6. Design curves of the fifth-order filter with a controllable imaginary frequency transmission zero pair correspond to various fractional bandwidth with $k = 1.56$.

of k , the bandwidth can be varied with corresponding change of ripple factor ε (return loss level). The design curves corresponding to various fractional bandwidth with $k = 1.56$ are shown in Fig. 6. From Fig. 6, the lower impedances Z_1 , Z_2 and Z_3 are, the wider passband bandwidth and the worse the return loss level could be achieved.

On the other hand, if a broader bandwidth is required without degrading the return loss, the only way is to increase the order of the filter. The S-parameters of the fifth- and seventh-order filter with the same return loss of 20.20 dB and the k value of 1.56 are shown in Fig. 7. It shows the passband bandwidth of the seventh-order filter can be extended about 14% with respect to the fifth-order filter.

B. Design Example of the Filter With a Controllable Transmission Pair on the Real Frequency

The second design example considers a wideband bandpass filter with the following specifications.

- 1) The fifth-order Chebyshev response with two transmission zeros on the real frequency.
- 2) Center frequency, ω_0 : 3 GHz
- 3) Passband bandwidth, W : 3 GHz
- 4) Stopband attenuation bump, A_{\min} , is lower than -20 dB

The circuit configuration of the fifth-order filter is shown in the first column of Table II. Again, in the first step, the even- and odd-mode analysis is adopted to calculate the S-parameters of the circuit. The even- and odd-mode eigennetworks are shown in

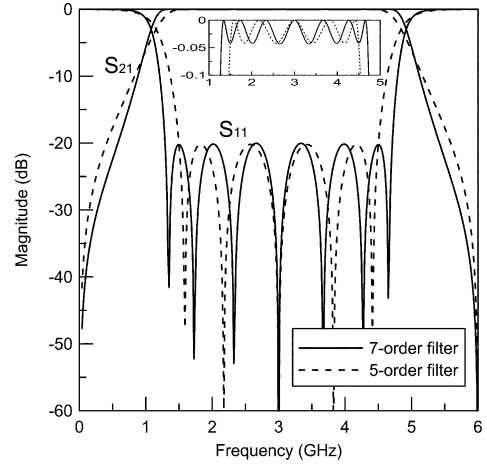


Fig. 7. S-parameters of the fifth- and seventh-order filter with the same return loss level.

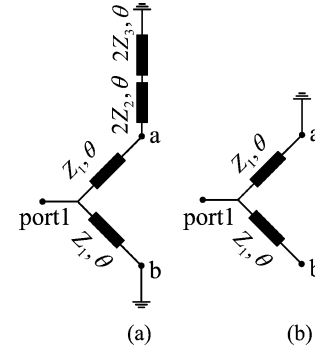


Fig. 8. (a) Odd-mode and (b) even-mode eigennetwork of the fifth-order filter with a controllable real frequency transmission zero pair.

Fig. 8, and the reflection coefficients for the even- and odd-mode eigennetworks are obtained as

$$\Gamma_{\text{even}} = \frac{1 - jz_1 t - t^2}{-1 - jz_1 t + t^2} \quad (32)$$

$$\Gamma_{\text{odd}} = \frac{[-j2z_2(z_1 + z_2 + z_3) - z_1 z_2(z_1 + 2z_2 + 2z_3)] \cdot t + j2[z_1 z_3 + z_2(z_2 + z_3)] \cdot t^2 + z_1^2 z_3 t^3}{[j2z_2(z_1 + z_2 + z_3) - z_1 z_2(z_1 + 2z_2 + 2z_3)] \cdot t - j2[z_1 z_3 + z_2(z_2 + z_3)] \cdot t^2 + z_1^2 z_3 t^3} \quad (33)$$

where $t = \tan \theta$ and z_1, z_2 and z_3 are the normalized impedance of Z_1, Z_2 and Z_3 . Using (1) and (2), we have the S-parameters of the filter shown in (34) and (35) on the bottom of this page. By solving $S_{21}^{\text{cir}} = 0$, the roots are as follows:

$$\tan \theta_z = \{0, j, -j, \sqrt{k}, -\sqrt{k}\} \text{ where } k = \frac{z_2}{z_3}. \quad (36)$$

$$S_{11}^{\text{cir}} = \frac{[j2(z_1 + z_2 + z_3) + j[z_1^2 z_2 - 2(z_2 + z_3)(z_1 + 2z_2 + z_1^2 z_2)] \cdot t^2 + j[z_1 z_3(z_1^2 - 2) - 2z_2(z_2 + z_3)] \cdot t^4]}{[-j2z_2(z_1 + z_2 + z_3) + z_1 z_2[3z_1 + 4(z_2 + z_3)] \cdot t - j[z_2(z_1^2 + 2)(z_1 + 2z_2 + 2z_3) + 2z_1 z_3] \cdot t^2]} \quad (34)$$

$$S_{21}^{\text{cir}} = \frac{z_1^2 z_2 t + z_1^2(z_2 - z_3) \cdot t^3 - z_1^2 z_3 t^5}{[-j2z_2(z_1 + z_2 + z_3) + z_1 z_2[3z_1 + 4(z_2 + z_3)] \cdot t - j[z_2(z_1^2 + 2)(z_1 + 2z_2 + 2z_3) + 2z_1 z_3] \cdot t^2]} \quad (35)$$

In the second step, according to the design specifications, the scaling factor and frequency mapping function can be acquired. The scaling factor δ is calculated to be 1 from (8). Therefore, the mapping function (9) can be expressed as

$$\Omega = -(\tan \theta)^{-1}. \quad (37)$$

By using of (10) and (36), the finite-frequency transmission zeros in the lowpass domain can be obtained as

$$\Omega_Z = \left\{ \frac{1}{j}, \frac{1}{-j}, \frac{1}{\sqrt{k}}, \frac{1}{-\sqrt{k}} \right\}. \quad (38)$$

It is observed in (38) that impedance ratio k determines the positions of a pair of real frequency transmission zeros.

In the third step, adopting the Cameron's method with zero locations in (38), the polynomials $P(\Omega)$ and $F(\Omega)$ can be obtained as follows:

$$P(\Omega) = -\frac{1}{k} + \frac{k-1}{k}\Omega^2 + \Omega^4 \quad (39)$$

$$F(\Omega) = \frac{C'(k)}{A'(k)} \cdot \Omega + \frac{B'(k)}{A'(k)} \cdot \Omega^3 + \Omega^5 \quad (40)$$

where

$$A'(k) = 11.67 - 5.83k + 11.67\sqrt{1-k} \quad (41)$$

$$B'(k) = -13.49 + 3.83k - 13.66\sqrt{1-k} \quad (42)$$

$$C'(k) = 3.83 + 2\sqrt{1-k}. \quad (43)$$

After the frequency mapping, (39) and (40) can be translated to the bandpass domain as

$$P(t) = -\frac{1}{k} + \frac{k-1}{k} \cdot \frac{1}{t^2} + \frac{1}{t^4} \quad (44)$$

$$F(t) = \frac{C'(k)}{A'(k)} \cdot \frac{1}{t} + \frac{B'(k)}{A'(k)} \cdot \frac{1}{t^3} + \frac{1}{t^5}. \quad (45)$$

In the fourth step, by (17), (18), (44) and (45), the two equal-ripple approximating functions can be illustrated as (46) and (47) as shown on the bottom of this page.

From (14), a polynomial equation can be obtained. Again, this polynomial equation is with variable t and each coefficient of the polynomial is a function of impedances and ripple factor ε . Setting each coefficient to be zero, we have following set of equations in (48), as shown at the bottom of this page.

According to (38) and (48), when the impedance ratio k is given, the impedances $Z_1Z_2Z_3$, the controllable transmission

TABLE IV
THREE POSSIBLE ANALYTICAL SOLUTIONS OF THE FIFTH-ORDER FILTER WITH A CONTROLLABLE REAL FREQUENCY TRANSMISSION ZERO PAIR

k	Ω_Z	Z_1 (Ohm)	Z_2 (Ohm)	Z_3 (Ohm)	ε	L_R (dB)
0.44	± 1.5	73.68	15.43	35.08	2.29	24.88
0.25	± 2	78.03	24.63	98.53	3.30	27.82
0.16	± 2.5	80.14	30.29	189.31	4.67	29.07

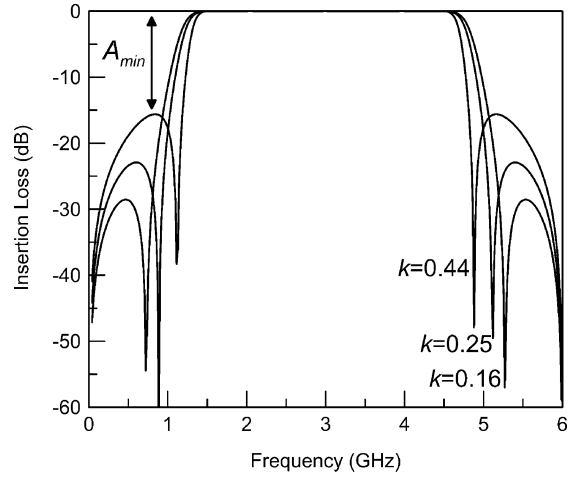


Fig. 9. Predicted stopband suppression under varied impedance ratio k .

zero pair Ω_Z , ripple factor ε and stopband attenuation bump A_{min} can be obtained. Table IV depicts three solutions corresponding to different k values. The insertion loss response of each solution in Table IV is represented in Fig. 9. From Fig. 9, the stopband attenuation bump is -22.9 dB when adopting the second solution $k = 0.25$. Again, for a fixed value of k , the bandwidth can be changed with associated change of stopband attenuation bump. Shown in Fig. 10 are the design curves corresponding to k value of 0.25. It is obvious in Fig. 10 that the lower impedance Z_1, Z_2 and Z_3 are, the wider passband bandwidth and the worse return loss and stopband attenuation bump could achieve.

Similarly, to keep return loss and k value the same, increasing the order of the filter increases the bandwidth of it. There gives an example. The S-parameters of the fifth- and seventh-order filter with the same return loss of 27.82 dB and k value of 0.25

$$\frac{S_{11}^{cir}(t)}{j \cdot S_{21}^{cir}(t)} = \frac{[2(z_1 + z_2 + z_3) + [z_1^2 z_2 - 2(z_2 + z_3)(z_1 + 2z_2 + z_1^2 z_2)]] \cdot t^2 + [z_1 z_3 (z_1^2 - 2) - 2z_2(z_2 + z_3)] \cdot t^4}{z_1^2 z_2 t + z_1^2 (z_2 - z_3) \cdot t^3 - z_1^2 z_3 t^5} \quad (46)$$

$$\frac{S_{11}(t)}{S_{21}(t)} = \frac{k\varepsilon A(k) + k\varepsilon B(k) \cdot t^2 + k\varepsilon C(k) \cdot t^4}{kA(k) \cdot t + (k-1)A(k) \cdot t^3 - A(k) \cdot t^5} \quad (47)$$

$$\begin{cases} 2z_1 + 2(k+1)z_3 - z_1^2 \varepsilon = 0 \\ A'(k) \cdot \{4z_1 - kz_1^3 + 2(1+k)^2 z_3 + [(k-1)\varepsilon - 2k(k+1)z_3]z_1^2\} + k\varepsilon z_1^2 \cdot B'(k) = 0 \\ A'(k) \cdot \{2(k^2 - 1)[k(z_1^2 - 1)z_3 - z_1] + k[(k-2)z_1 + \varepsilon]z_1^2\} - k \cdot [(k-1)B'(k) + kC'(k)] \cdot \varepsilon z_1^2 = 0 \end{cases} \quad (48)$$

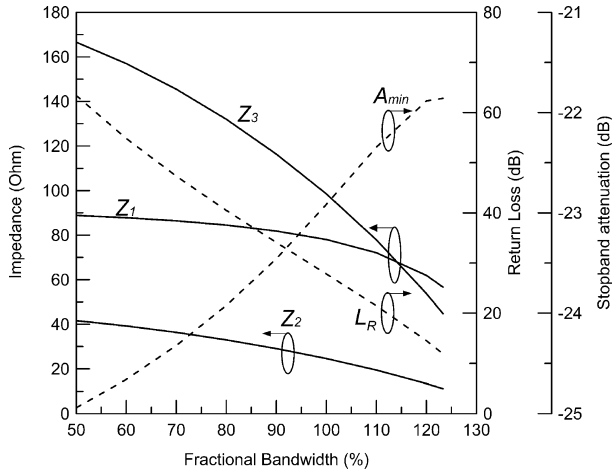


Fig. 10. Design curves corresponding to $k = 0.25$.

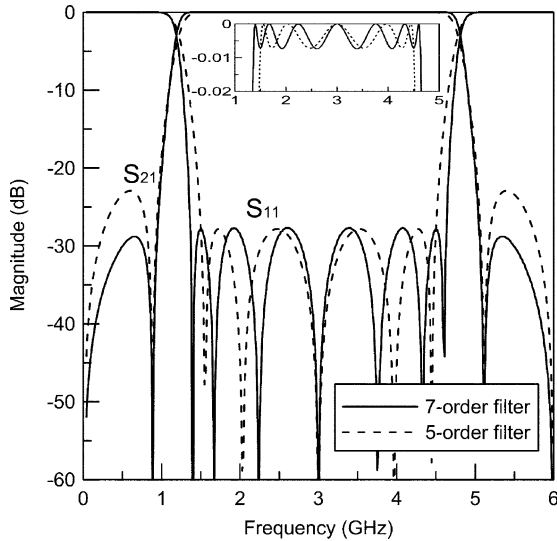


Fig. 11. S-parameters of the fifth- and seventh-order filter with return loss of 27.82 dB and k value of 0.25.

are shown in Fig. 11. In Fig. 11, the passband bandwidth of the seventh-order filter is about 10% larger than that of the fifth-order filter.

IV. REALIZATION AND MEASUREMENT OF PROPOSED FILTERS

The finite ground coplanar waveguide and coplanar stripline are chosen to implement the filters because both of them are easy to realize a large range of impedance values and possible to realize a phase inverter. The circuits are implemented on an Al_2O_3 substrate with a dielectric constant of 9.8 and thickness of 15 mil. The circuit side of the substrate is deposited with 1.5- μm -thick gold film.

A. Experimental Results of the Filter With a Controllable Transmission Zero Pair on the Imaginary Frequency

The fifth-order filter with a k value of 1.56, a return loss of 20.2 dB, a Z_1 of 67.88 Ω , a Z_2 of 46.31 Ω , a Z_3 of 72.36 Ω , and a passband of 1.50 to 4.5 GHz (100% fractional bandwidth) is realized. Fig. 12(a) shows the circuit photo of the filter. In Fig. 12(a), the ring is implemented by coplanar stripline and the

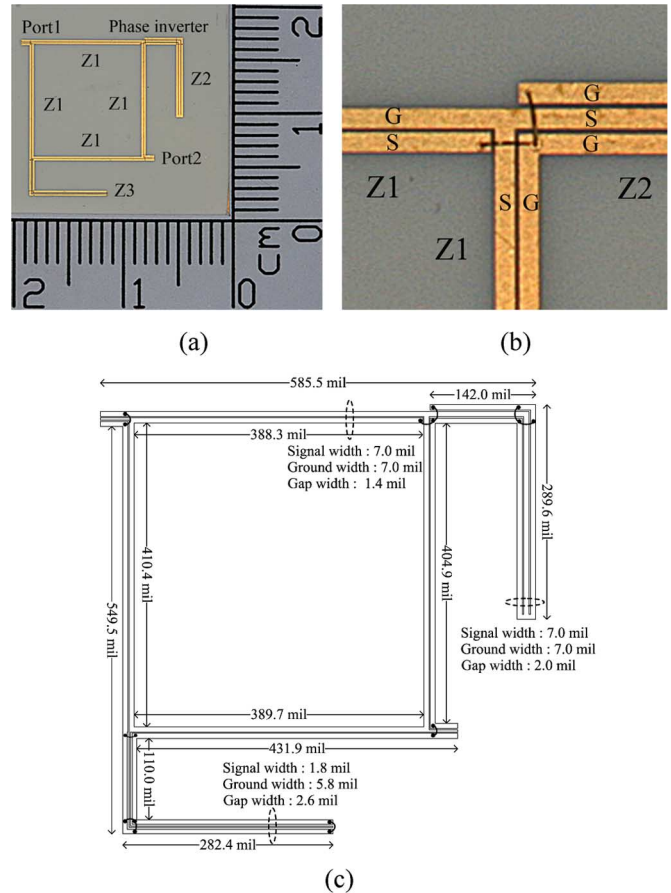


Fig. 12. Circuit photos and layout of the fifth-order filter with a controllable imaginary frequency transmission zero pair. (a) the whole circuit, (b) the phase inverter and (c) the schematic layout.

I/O ports and stubs are implemented by finite ground coplanar waveguide. The phase inverter is formed by twist-connected finite ground coplanar waveguide and coplanar stripline [22] as shown in Fig. 12(b).

Fig. 13 depicts the theoretical, measured and EM simulated S-parameters of the proposed filter. The measured passband insertion loss is approximately 2.4 dB. The measured 10-dB return loss bandwidth is from 1.35 to 4.90 GHz (118.3%). However, the thin gold film causes larger passband insertion loss. The insertion loss can be improved by increasing the metal thickness. Fig. 14 illustrates the theoretical, measured and EM simulated group delay of the proposed filter. The in-band group delay is about 0.45 ns that is very flat and matches well with the calculated result.

B. Experimental Results of the Filter With a Controllable Transmission Zero Pair on the Real Frequency

The fifth-order filter with a k value of 0.25, a return loss of 27.8 dB, a hybrid ring impedance Z_1 of 78.04 Ω , the two-section short-circuited stub impedances Z_2 of 24.63 Ω and Z_3 of 98.53 Ω , a passband of 1.50 to 4.5 GHz (100% fractional bandwidth), and a stopband attenuation bump of -22.9 dB is also fabricated on an Al_2O_3 substrate. A photograph of the fabricated filter is shown in Fig. 15(a). Similarly, the ring is implemented by coplanar stripline and the stub and I/O ports are realized by finite ground coplanar waveguide. Again, the phase inverter is

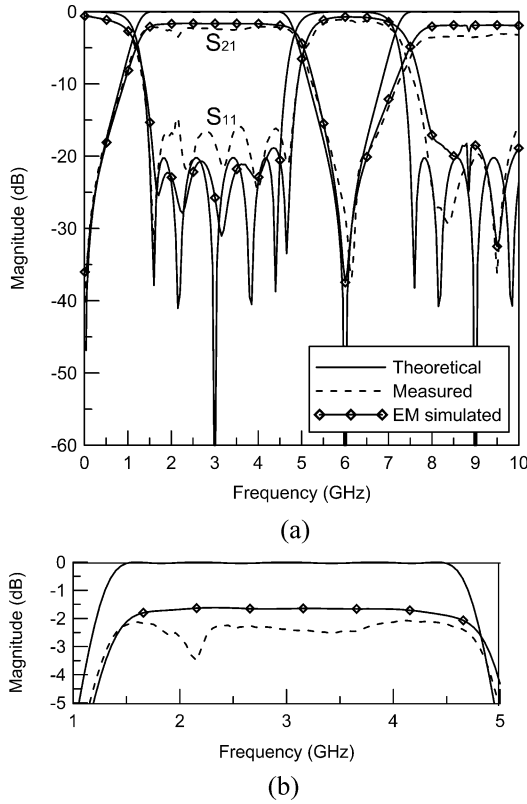


Fig. 13. Theoretical, measured and EM simulated S parameters of the fifth-order filter with a controllable imaginary frequency transmission zero pair. (a) wideband frequency response, and (b) closer look in the passband response.

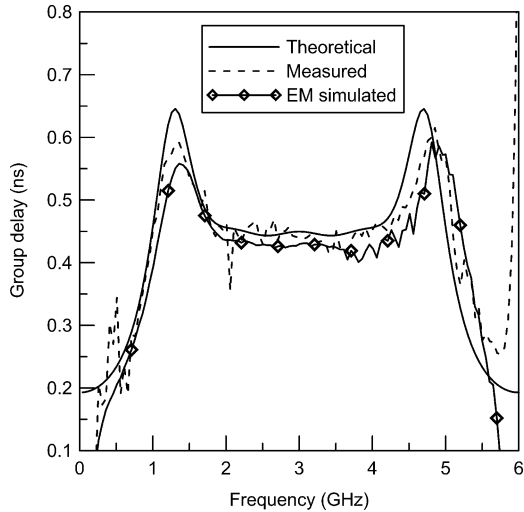


Fig. 14. Theoretical, measured and EM simulated group delay of the fifth-order filter with a controllable imaginary frequency transmission zero pair.

implemented by twist-connected coplanar stripline and finite ground coplanar waveguide as illustrated in Fig. 15(b). It can be found in Fig. 15(b) that the 24.63Ω finite ground coplanar waveguide is formed by two parallel-connected finite ground coplanar waveguide lines.

Fig. 16 demonstrates the theoretical, measured and EM measured results of the proposed filter and the measured passband insertion loss is approximately 1.3 dB. The measured 10-dB return loss bandwidth is from 1.25 to 4.68 GHz (114.3%). The insertion loss in the passband also can be improved by increasing

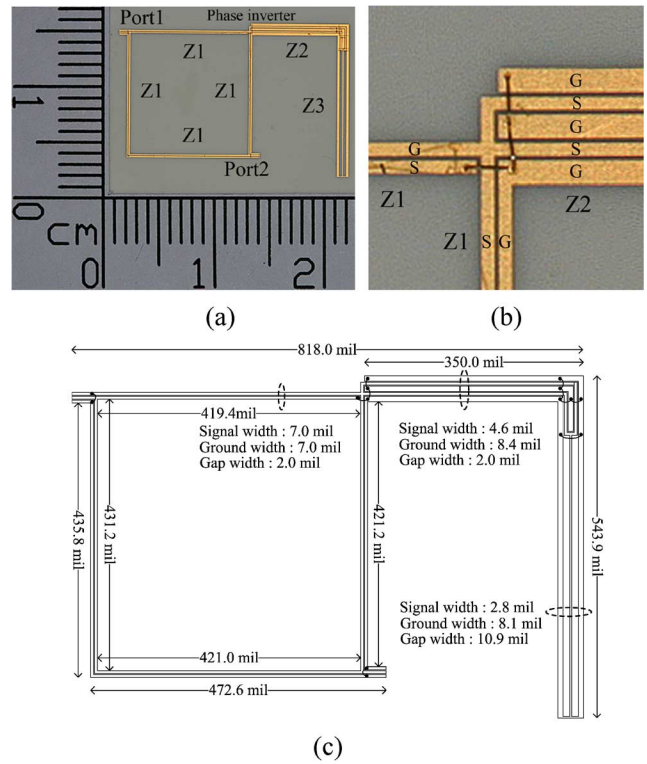


Fig. 15. Photograph and layout of the fabricated fifth-order filter with a controllable real frequency transmission zero pair.

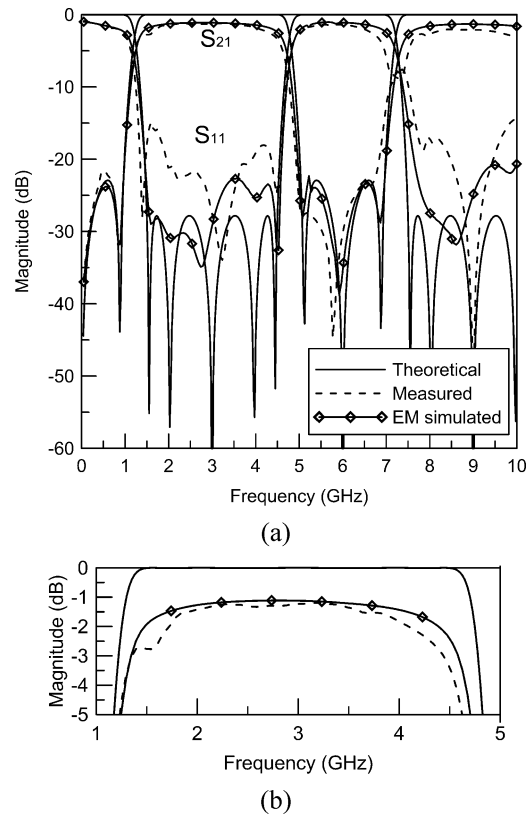


Fig. 16. Theoretical, measured and EM simulated S parameters of the fifth-order filter with a controllable real frequency transmission zero pair. (a) wideband frequency response, and (b) closer look in the passband response.

the metal thickness. Besides, the fabrication variation of line impedances and the extra phase delay introduced by the bonding

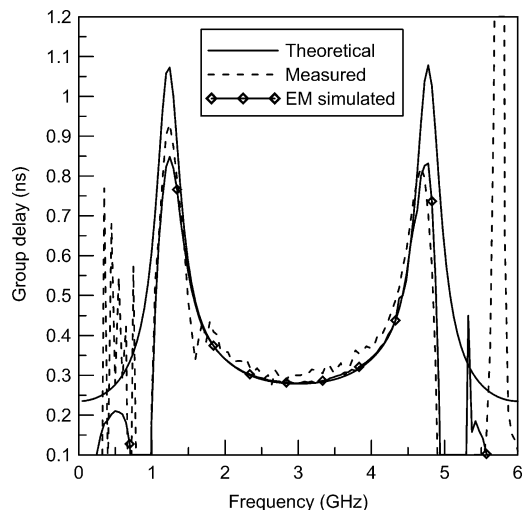


Fig. 17. Theoretical, measured and EM simulated group delay of the fifth-order filter with a controllable real frequency transmission zero pair.

wires of the phase inverter should cause the asymmetrical low-side and high-side stopband attenuation bump. Fig. 17 depicts the theoretical, measured and EM simulated group delay of the proposed filter. The in-band group delay is typically 0.3 ns and it matches well with the calculated result. It can be found in Fig. 14 and 17 that the flatness of in-band group delay of the filter with a controllable transmission zero pair on the real frequency is worse than that of the filter with a controllable transmission zero pair on the imaginary frequency.

V. CONCLUSION

In this paper, the hybrid ring with a multi-section short-circuited stub and a multi-section open-circuited stub has been proposed to implement two novel kinds of wideband bandpass filters with generalized Chebyshev response. The filter with a controllable transmission zero pair on the imaginary frequency can be designed for the maximum flat group delay while the filter with a controllable transmission zero pair on the real frequency can be designed for improving the stopband suppression. Meanwhile, the corresponding synthesis method is also developed to explicitly determine the impedances, ripple factor and return loss of the proposed filters under the required specifications. Finally, two design examples, a fifth-order filter with a controllable imaginary frequency transmission zero pair and a fifth-order filter with a controllable real frequency transmission zero pair, were fabricated and measured. The coplanar stripline and finite ground coplanar waveguide have been successfully applied to implement the filters. The measured results evidently confirmed the validity of the proposed structures as well as the synthesis methodology. A design flow chart has provided the designers with an efficient way in design and exploration of two kinds of the proposed wideband bandpass filters.

REFERENCES

- [1] Y. S. Lin, W. C. Ku, C. H. Wang, and C. H. Chen, "Wideband coplanar-waveguide bandpass filters with good stopband rejection," *IEEE Microw. Wireless Compon. Lett.*, vol. 14, no. 9, pp. 422–424, Sep. 2004.
- [2] C. L. Hsu, F. C. Hsu, and J. T. Kuo, "Microstrip bandpass filter for ultra-wideband (UWB) wireless communications," in *IEEE MTT-S Int. Microw. Symp. Dig.*, Jun. 2005, pp. 679–682.

- [3] J. T. Kuo and E. Shih, "Wideband bandpass filter design with three-line microstrip structures," *IET Microwave, Antennas Propag.*, vol. 149, no. 516, pp. 243–247, Oct./Dec. 2002.
- [4] L. Zhu, H. Bu, and K. Wu, "Aperture compensation technique for innovative design of ultra-broadband microstrip bandpass filter," in *IEEE MTT-S Int. Microw. Symp. Dig.*, 2000, pp. 315–318.
- [5] L. Zhu, S. Sun, and W. Menzel, "Ultra-wideband (UWB) bandpass filters using multiple-mode resonator," *IEEE Microw. Wireless Compon. Lett.*, vol. 15, no. 11, pp. 796–798, Nov. 2005.
- [6] S. Sun and L. Zhu, "Multiple-mode-resonator-based bandpass filters for ultra wideband transmission systems," *IEEE Microw. Mag.*, vol. 10, no. 2, pp. 88–98, Apr. 2009.
- [7] P. Cai, Z. Ma, X. Guan, Y. Kobayashi, T. Anada, and G. Hagiwara, "A novel compact ultra-wideband bandpass filter using a microstrip stepped-impedance four-modes resonator," in *Proc. IEEE MTT-S Int. Microw. Symp. Dig.*, Jun. 2007, pp. 751–754.
- [8] L. H. Hsieh and K. Chang, "Compact, low insertion-loss, sharp-rejection, and wideband microstrip bandpass filters," *IEEE Trans. Microw. Theory Tech.*, vol. 51, no. 4, pp. 1241–1246, Apr. 2003.
- [9] H. Ishida and K. Araki, "Design and analysis of UWB bandpass filter with ring filter," in *Proc. IEEE MTT-S Int. Microw. Symp. Dig.*, Jun. 2004, vol. 3, pp. 1307–1310.
- [10] W. Liu, Z. Ma, C. P. Chen, G. Zheng, and T. Anada, "A novel UWB filter using a new type of microstrip double-ring resonators," in *Proc. Asia-Pacific Microw. Conf.*, Dec. 2006, pp. 33–36.
- [11] S. Sun and L. Zhu, "Wideband microstrip ring resonator bandpass filters under multiple resonances," *IEEE Trans. Microw. Theory Tech.*, vol. 55, no. 10, pp. 2176–2182, Oct. 2007.
- [12] C. H. Chi and C. Y. Chang, "A wideband bandpass filter with wide upper stopband using stepped-impedance cascaded 180° hybrid rings," *IEEE Microw. Wireless Compon. Lett.*, vol. 17, no. 8, pp. 589–591, Aug. 2007.
- [13] R. Gomez-Garcia and J. I. Alonso, "Systematic method for the exact synthesis of ultra-wideband filtering responses using high-pass and low-pass sections," *IEEE Trans. Microw. Theory Tech.*, vol. 54, no. 10, pp. 3751–3764, Oct. 2006.
- [14] R. Li, S. Sun, and L. Zhu, "Synthesis design of Ultra-wideband bandpass filters with composite series and shunt stubs," *IEEE Trans. Microw. Theory Tech.*, vol. 57, no. 3, pp. 684–692, Mar. 2009.
- [15] P. Cai, Z. Ma, X. Guan, Y. Kobayashi, T. Anada, and G. Hagiwara, "Synthesis and realization of novel ultra-wideband bandpass filters using 3/4 wavelength parallel-coupled line resonators," in *Proc. Asia-Pacific Microw. Conf.*, Dec. 2006, pp. 159–162.
- [16] H. J. Riblet, "The application of a new class of equal-ripple functions to some familiar transmission-line problems," *IEEE Trans. Microw. Theory Tech.*, vol. 12, pp. 415–421, Jul. 1964.
- [17] R. Levy and L. F. Lind, "Synthesis of symmetrical branch-guide directional couplers," *IEEE Trans. Microw. Theory Tech.*, vol. 16, no. 2, pp. 80–89, Mar. 1968.
- [18] M. C. Horton and R. J. Wenzel, "General theory and design of optimum quarter-wave TEM filters," *IEEE Trans. Microw. Theory Tech.*, vol. 13, no. 3, pp. 316–327, Mar. 1965.
- [19] H. J. Carlin and W. Kohler, "Direct synthesis of bandpass transmission line structures," *IEEE Trans. Microw. Theory Tech.*, vol. 13, no. 5, pp. 283–297, Mar. 1965.
- [20] R. J. Cameron, "General coupling matrix synthesis methods for Chebyshev filtering functions," *IEEE Trans. Microw. Theory Tech.*, vol. 47, no. 4, pp. 433–442, Apr. 1999.
- [21] D. Swanson and G. Macchiarella, "Microwave filter design by synthesis and optimization," *IEEE Microw. Mag.*, vol. 8, no. 2, Apr. 2007.
- [22] C. Y. Chang and C. C. Yang, "A novel broadband Chebyshev-response rat-race ring coupler," *IEEE Trans. Microw. Theory Tech.*, vol. 47, no. 4, pp. 455–462, Apr. 1999.



components design.

Jian-Yu Li (S'07) was born in Pingtung, Taiwan. He received the B.S.E.E. and M.S.E.E. degrees from the National Sun Yat-Sen University, Kaohsiung, Taiwan, in 1998 and 2000, respectively, and is currently working toward the Ph.D. degree in communication engineering at the National Chiao Tung University, Hsinchu, Taiwan.

In 2000, he joined Information and Communications Research Laboratories, ITRI, Hsinchu, Taiwan, R.O.C., as an engineer. His research interests are in the area of microwave integrated circuits and passive



packages.

Chun-Hsiang Chi was born in Kaohsiung, Taiwan, on August 13, 1980. He received the B.S. degree in electrical engineering from the National Sun Yat-Sen University, Kaohsiung, Taiwan, in 2002, and the M.S. degree and Ph.D. degree in communication engineering from the National Chiao Tung University, Hsinchu, Taiwan, in 2004 and 2009, respectively.

In 2009, he joined Information and Communications Research Laboratories, ITRI, Hsinchu, Taiwan, as an Engineer. His research interests are in the area of microwave and millimeter-wave circuits and



Chi-Yang Chang (S'88–M'95) was born in Taipei, Taiwan, on December 20, 1954. He received the B.S. degree in physics and M.S. degree in electrical engineering from the National Taiwan University, Taipei, Taiwan, in 1977 and 1982, respectively, and the Ph.D. degree in electrical engineering from the University of Texas at Austin, in 1990.

From 1979 to 1980, he was with the Department of Physics, National Taiwan University, as a Teaching Assistant. From 1982 to 1988, he was with the Chung-Shan Institute of Science and Technology (CSIST), as an Assistant Researcher, where he was in charge of development of microwave integrated circuits (MICs), microwave subsystems, and millimeter-wave waveguide E-plane circuits. From 1990 to 1995, he returned to CSIST as an Associate Researcher in charge of development of uniplanar circuits, ultra-broadband circuits, and millimeter-wave planar circuits. In 1995, he joined the faculty of the Department of Electrical Engineering, National Chiao-Tung University, Hsinchu, Taiwan, as an Associate Professor and became a Professor in 2002. His research interests include microwave and millimeter-wave passive and active circuit design, planar miniaturized filter design, and monolithic-microwave integrated-circuit (MMIC) design.